Ion mobility mass spectrometry enables the discrimination of positional isomers and the detection of conformers from cyclic oligosaccharides-metals supramolecular complexes

Véronique Bonnet, Gilles Clodic, Christian Sonnendecker, Wolfgang Zimmermann, Cédric Przybylski

Ion mobility mass spectrometry enables the discrimination of positional isomers and the detection of conformers from cyclic oligosaccharides-metals supramolecular complexes

Véronique Bonnet[a], Gilles Clodic,[b] Christian Sonnendecker,[c] Wolfgang Zimmermann,[c] and Cédric Przybylski*[d,e]

[a] Laboratoire de Glycochimie, des Antimicrobiens et des Agroressources, Université de Picardie Jules Verne, 80039 Amiens, France.

[b] Sorbonne Université, Mass Spectrometry Sciences Sorbonne University, MS3U Platform, UFR 926, UFR 927, Paris, France.

[c] Institute of Analytical Chemistry, Leipzig University, 04103 Leipzig, Germany.

[d] Sorbonne Université, CNRS, Institut Parisien de Chimie Moléculaire, IPCM, 4 Place Jussieu, 75005 Paris, France.

[e] Université Paris-Saclay, Univ Evry, CNRS, LAMBE, Evry-Courcouronnes, 91000, France.

Email: cedric.przybylski@univ-evry.fr

ABSTRACT

Cyclic oligosaccharides are well known to interact with various metals, able to form supramolecular complexes with distinct sizes and shapes. However, the presence of various isomers in a sample, including positional isomers and conformers, can significantly impact molecular recognition, encapsulation ability and chemical reactivity. Therefore, it is crucial to have tools for deep samples probing and correlation establishments. The emerging ion mobility mass spectrometry (IM-MS) has the advantages to be rapid and sensitive, but is still in its infancy for the investigation of supramolecular assemblies. In the herein study, it was demonstrated that IM-MS is suitable to discriminate several isomers of cyclodextrins (CD)-metals complexes, used as cyclic oligosaccharide models. In this sense, we investigated branched 6-O-α-glucosyl- or 6-O-α-maltosyl-β-cyclodextrins (G_1-β-CD and G_2-β-CD) and their purely cyclic isomers: CD8 (γ-CD) and CD9 (δ-CD). The corresponding collision cross section (CCS) values were deducted for the main positive singly and doubly charged species. Experimental CCS values were matched with models obtained from molecular modelling. The high mobility resolving power and resolution enabled discrimination of positional isomers, identification of various conformers and accurate relative content estimation. These results represent a milestone in the identification of carbohydrate conformers that cannot be easily reached by other approaches.

Keywords: Cyclic oligosaccharides; Cyclodextrins; Conformers; Isomers; Supramolecular assembly; Ion-mobility.

1. INTRODUCTION

With cellulose, starch is among the most abundant polysaccharides present in the nature (Tester et al., 2004). Various bacterial enzymes such as α-amylase and cyclodextrin glycosyltransferase (CGTases), are able to degrade starch to produce lower size molecules i.e. oligosaccharides. Indeed, the aforementioned enzymes own unique capacity to catalyse the formation of α(1→4) malto-oligosaccharides as linear (maltodextrins), but also circular ones (cyclodextrins; CDs). CDs are formed by the enzymatic conversion of polysaccharide by CGTases through intramolecular transglycosylation reaction, leading mainly to CDs with 6 (α-CD), 7 (β-CD), or 8 (γ-CD) α(1→4) linked D-glucopyranose units (Glc) as final products. In spite of these last ones, which are commercially available and have been extensively investigated,(Szejtli, 1998) it was reported that CDs with higher degree of polymerization (DP) (until >100) can be also obtained. Nonetheless, larger CDs (DP ≥9) are rapidly degraded by the enzyme in a reverse reaction to linear glucans which are subsequently converted to α-, β- and γ-CD, leading to a negligible yield of the larger ones (Sonnendecker, Melzer, et al., 2019; Sonnendecker, Thürmann, et al., 2019; Terada et al., 1997; Terada Yoshinobu et al., 2001; M. Zheng et al., 2002). However, elegant approaches dealing with the templated enzymatic synthesis to promote some CD sizes have been very recently described (Erichsen et al., 2023; Samuelsen et al., 2022; Yang et al., 2021). Furthermore, incomplete depolymerisation/cyclization processes can also lead to branched α-glycosylated-(1→6)CD (Ao et al., 2007; D. French et al., 1965; Taniguchi & Honnda, 2009; Terada et al., 1997). The main interest of CDs is based on their structure/properties relationship where they exhibit a doughnut shape with a hydrophobic cavity able to reversibly encapsulate several organic molecules (Kfoury et al., 2018;

Song et al., 2009), and disclose peripherally hydrophilic features that form an intra- and inter-hydrogen bonding network (Loftsson et al., 2005). Such properties drive the particularly attractive roles of CDs in several fields like food, pharmaceutical and cosmetic industries (Singh et al., 2002).

The efficiency of supramolecular host-guest complexes is tightly dependent on the structure of the host molecule, though if presence of CDs with (bio)chemical modifications can be easily discriminated, the differentiation of isomeric forms of unmodified CDs can be a more challenging task. In this sense, the first bottleneck is to achieve an acceptable separation to unambiguously identify each species. Liquid chromatography (LC) was employed to achieve this, yielding contrasting outcomes. Hence, some partial separation was reached for positional isomers of diglucosyl-β-CD ($(G_1)_2$-β-CD), maltotriosyl-β-CD (G_3-β-CD) (Koizumi et al., 1991; Okada et al., 1994), or also heterogeneous doubly branched α-D-galactosyl-/α-D-glucosyl-α-CD (Koizumi et al., 1986). On the other hand, complete separation was achieved in one run for positional isomers of di-α-D-glucosyl-γ-CD ($(G_1)_2$-γ-CD) (Koizumi et al., 1986; Tanimoto et al., 1995), as well as with a mixture of β-CD, α-CD, G_1-β-CD, G_2-β-CD and $(G_2)_2$-β-CD (Yamamoto et al., 1989), or with two distinct columns for α-, β- or γ-CD and their maltosyl grafted derivatives (Shiraishi et al., 1989). ^{1}H or ^{13}C NMR was also successfully applied to characterize α-CDs and 6-O-α-glucopyranosyl- to 6-O-α-maltoheptaosyl-α-CD (G_1-α-CD to G_7-α-CD) (Ishizuka et al., 2004), as well as for doubly and triply branched glucosyl-CDs ($(G_1)_2$/$(G_1)_3$-γ-CD) (Koizumi et al., 1986, 1990, 1991; Tanimoto et al., 1995), maltosyl-CD (Abe et al., 1988; Okada et al., 1994), or longer branched glucosyl chains.(Hizukuri et al., 1989) While mass spectrometry (MS) is commonly used for the characterization of cyclodextrins (CDs), there are relatively few studies that have focused on the analysis of their glycosyl

derivatives. Fast Atom Bombardment MS was applied for masses verification of glucosyl- to maltopentaosyl-α-CD (Hizukuri et al., 1989) or also various isomers of doubly branched β-CD (Abe et al., 1988; Koizumi et al., 1986, 1991). MS spectrum of G_2-β-CD (Yamamoto et al., 1989), was also obtained by Secondary Ionization MS (SIMS), while electrospray coupled to quadrupole-time-of-flight (ESI-QTOF) instrument was successfully used for MS/MS of G_1-β-CD (Xia et al., 2017). Yamagaki *et al*. reported the possibility to associate the relative intensities of fragment ions issued from the post-source decay (PSD) in MALDI-TOF MS with the chemical structures of three CD isomers, namely γ-CD, G_2-α-CD and $(G_1)_2$-α-CD (Yamagaki et al., 1996). The correlation seems to be caused by the difference in the number of cleavage sites at the glycosidic bond. It was found that the intensity of the PSD ion resulting from one cleavage is higher than that resulting from two cleavages at this linkage. It can be hypothesized that energy is more widely dissipated in the latter case. The same authors have also given evidence that measurements at a reduced acceleration voltage were advantageous to distinguish easily between the otherwise very similar PSD fragment spectra of G_1-β-CD and $(G_1)_2$-α-CD (Yamagaki & Nakanishi, 1999). More recently, it has been demonstrated that two isomers of larger CD i.e. CD10 and G_1-CD9 can be distinguished by a characteristic loss of 120.04 mass units. That corresponds to $^{0,2}X_1$ cross ring cleavage of a grafted non-reducing end (1→6) glucosyl unit, and obtained from higher energy collision dissociation (HCD) MS/MS step (Sonnendecker, Thürmann, et al., 2019). However, none of these aforementioned approaches allows both a direct discrimination of such CD isomers and a sub-milligram sample consumption.

During the last decade, a promising approach named ion mobility-MS (IM-MS) has been more widely introduced and could overcome previously described limitations. IM-MS is a 2D method, that is suitable to resolve glycan isomers (Bansal et al., 2020; Clowers et al., 2005; Gabryelski & Froese, 2003; Gaye et al., 2015; Harvey et al., 2018; Hofmann et al., 2015; Huang & Dodds, 2013; Li et al., 2013; Nagy et al., 2018; Przybylski & Bonnet, 2021; Pu et al., 2016; Rashid et al., 2014; Xie et al., 2021; X. Zheng et al., 2017). During IM-MS, the ions are separated not only according to their m/z, but also as function of their size and shape in the gas phase, which is portrayed by collision cross section (CCS) values in a given gas. IM-MS has been successfully applied to the characterization of a large variety of linear and branched saccharidic isomers using various technological setups such as field asymmetric ion mobility spectrometry (FAIMS) (Gabryelski & Froese, 2003), traveling wave ion mobility (TWIM) (Harvey et al., 2018; Hofmann et al., 2015; Huang & Dodds, 2013; Rashid et al., 2014), drift tube ion mobility spectrometry (DTIMS) (Clowers et al., 2005; Gaye et al., 2015; Li et al., 2013; X. Zheng et al., 2017), improved serpentine ion pathway like structures for lossless ion manipulation (SLIM) (Bansal et al., 2020; Nagy et al., 2018), or also trapped ion mobility spectrometry (TIMS) (Przybylski & Bonnet, 2021; Pu et al., 2016; Xie et al., 2021). Since the first report in 1997 by Clemmer and Liu of the first drift time for α-, β- and γ-CD and their fragments, only a few studies focusing on IM-MS of CD have been reported (Liu & Clemmer, 1997). α-, β- and γ-CD were analyzed by ESI-/MALDI-DTIMS (Fenn & McLean, 2011; Klein et al., 2018; S. Lee et al., 1997). More recently, ESI-TWIMS was successfully applied to study mono- to trimeric β-CD (Berland et al., 2014), as well as complexes involving α- and β-CD with either o-, m- or p-coumaric acids (Kralj et al., 2009), amino-β-CD/labile sesamins

(Sugahara et al., 2015), α- or β-CD with piperine or curcumin (Nag et al., 2018), whereas such analysis with same CDs based complexes and amino acids were also reported (Chen et al., 2018; S.-S. Lee et al., 2018). Ding and colleagues have demonstrated the potential to use TIMS for enantiomeric distinction of D/L amino acids by forming complexes with CDs and Mg^{2+} (Yang et al., 2022). Smith and colleagues have elegantly developed a coupling of TW-SLIM utilizing serpentine ultra-long path with extended routing (SUPER) for analysis of α-CD with bile acids in negative and positive modes (Chouinard et al., 2018). Yamagaki and colleagues showed, using TWIM-MS, that the drift times of γ-CD, G_2-α-CD and $(G_1)_2$-α-CD, and their product ions with the same masses were almost the same in collision-induced dissociation (CID) MS/MS (Yamagaki & Sato, 2009). In contrast, the IM peak widths were suggested to serve as 'trend line' to discriminate between the three isomers. Indeed, the IM peak widths were sensitive to structural differences of the isomeric product ions. For example, the product ions $[M\text{-}Glc_n+H]^+$ (n=0∼6) of γ-CD exhibited a linear correlation with their masses, whereas the product ions with larger and/or longer chains had broader peak widths (Yamagaki & Sato, 2009). Nevertheless, the aforementioned MS approaches only give partial and indirect information. Very recently, we successfully demonstrated the usefulness of ESI-TIMS-TOF to differentiate isomers of supramolecular complexes with tubular shape based on CDs with alkali metals (Przybylski & Bonnet, 2022). Moreover, with the same instrumentation Chakraborty *et al*. have fruitfully probed the isomerism of CD based oligomers with Cu^{2+} (Chakraborty et al., 2023).

In the present work, we hypothesize that high-resolution IM-MS such as ESI-TIMS-TOF can be suitable to discriminate CD isomers as well as to be compatible with the timescale of interconversion to unveil and quantify potential conformers. The ability of such high-resolution instrument to differentiate studied models of cyclic oligosaccharides according to their metal adduct, size, structure and shape feature was also investigated.

2. MATERIALS AND METHODS

2.1. Chemicals and Materials

γ-Cyclodextrin was kindly supplied by Wacker Chimie S.A.S (Lyon, France). 6-*O*-α-Maltosyl-β-cyclodextrin (G_2-β-CD), LiCl, NaCl, KCl, RbCl and CsCl alkali salts were purchased from Sigma-Aldrich (Saint-Quentin Fallavier, France). 6-*O*-α-D-Glucosyl-β-cyclodextrin (G_1-β-CD), was provided from ABCR Chemie. According to previously described procedures, large ring CD9 (δ-CD) was produced by action on starch of a specifically genetically engineered CGTase followed by LC purification steps as described elsewhere (Sonnendecker et al., 2017; Sonnendecker, Melzer, et al., 2019; Sonnendecker, Thürmann, et al., 2019). Methanol of MS grade used for sample preparation was purchased from VWR (West Chester, PA, USA). Water was of ultrapure quality.

2.2 Solvents

Methanol used for sample preparation was of MS grade and was purchased from VWR (West Chester, PA, USA). Water was of ultrapure quality (18.2 MΩ).

2.3 Samples

160 Stock solutions were made at 1 mM in water. Then, the solution was diluted to 1 µM in metha-
161 nol/water (1:1 v/v) with 0.3 µM of one given salt or a mixture of them for further analysis.

162 **2.4 TimsTOF™ experiments.**

163 An ESI-TIMS-TOF™ instrument (Bruker Daltonics, Bremen, Germany) operating with oTOF control
164 v5.0 software was used. The source temperature was held at 200°C, and the drying and nebuliz-
165 ing gas (N_2) operated at a flow rate of 3 L. min^{-1} and at a pressure of 0.3 bar, respectively. The
166 instrument was calibrated using Tuning Mix G24221 (Agilent Technologies, Les Ulis, France). Ap-
167 plied voltages were +4 kV and -0.5 kV for capillary and endplate offset, respectively. The acquisi-
168 tion was achieved in the *m/z* 300-4000 range with a centre at *m/z* 500. TIMS separation depends
169 on the gas flow velocity (v_g), elution voltage ($V_{elution}$), ramp time (t_{ramp}), base voltage (V_{out})
170 and the electric field $(\vec{E})$. The reduced mobility, K_0, can be calculated as follows (Eq. 1):

171 $$\mathrm{K_0} = \frac{v_g}{\vec{E}} = \frac{A}{(V_{elution} - V_{out})} \quad \text{(Eq. 1)}$$

172 The mobility calibration constant *A* was determined using known reduced mobilities of tuning
173 mix components. The resolving power (*R*) and resolution (*r*) are defined as $R = (1/\mathrm{K_0})/w$ and
174 $r = 1.18 \times [(1/\mathrm{K_0})_2 - (1/K_0)_1]/(w_1 + w_2)$, where *w* is the full peak width at half maximum.
175 To improve separation efficiency, the scan rate (*Sr*= $\Delta \mathrm{V_{ramp}}/\mathrm{t_{ramp}}$) was tuned by imeX™ tech-
176 nology. For this, t_{ramp} is automatically set as function of manually adjusted ΔV_{ramp}. N_2 was used
177 as buffer gas at funnel temperature (T = 305 K) with v_g set by the pressure difference of 1.69
178 mbar. A potential of 350 Vpp was applied to radially confine the trapped ion cloud. The measured

inverse reduced mobilities were converted into collision cross sections (CCS) using the Mason-Schamp equation (Eq. 2):

$$\Omega = \frac{(18\pi)^{1/2}}{16} \times \frac{q}{(k_B \times T)^{1/2}} \times \left[\frac{1}{m_i} + \frac{1}{m_g}\right]^{1/2} \times \frac{1}{N} \times \frac{1}{\mathrm{K}_0} \quad \text{(Eq. 2)}$$

where q is the ion charge, k_B is the Boltzmann constant, N is the gas number density, m_i is the ion mass, and m_g is the gas molecular mass. TIMS-MS spectra and mobilograms were analysed using Compass Data Analysis 5.1 (Bruker, Germany).

2.6 ESI-TIMS-MS analysis of the cyclo-oligosaccharides

Throughout this study, all cyclodextrins were analysed in the positive ion mode as singly or doubly charged ions with or without salt doping. All samples were continuously infused at 3 µL.min^{-1} via a 250 mL syringe. All experiments were performed in quintuplicate and were reproducible across the replica measurements.

2.7 Theoretical collision cross section calculations

All initial geometry relaxations were performed using the Merck molecular force field (MMFF94) implemented in Avogadro (v1.95.1). Geometry optimization was finalized using density functional theory (DFT) calculations with NWChem (v7.0). Theoretical CCS calculations were carried out in IMoS (v.1.10) (Larriba & Hogan, 2013) using the average of ten processes by Elastic/Diffuse Hard Sphere Scattering (EHSS/DHSS) or Trajectory method Diffuse Hard Sphere Scattering (DTHSS with 4-inf potential) (Wei et al., 2019).

3. RESULTS AND DISCUSSION

Cyclodextrins like most of the neutral carbohydrates exhibit a strong affinity for metals, especially alkali and (post-)transition ones (Przybylski et al., 2015; Dossmann et al., 2021). Such attachment is advantageously used to detect the cyclodextrin as a wide variety of ionic complexes with variable stoichiometries which can be summarized as $[nCD+mX]^{z+}$, where n is the number of cyclodextrins, m and X is the number and the studied metal, respectively, and z the number of charge. Due to its highly softness, ESI is the most suitable ionization method to transfer intact assemblies from solution to gas phase for MS analysis. ESI mass spectra showed numerous ions, as for example for G_2-β-CD dopped with salts mixture (Fig. 1) or γ-CD, G_1-β-CD and γ-CD (Fig. S1).

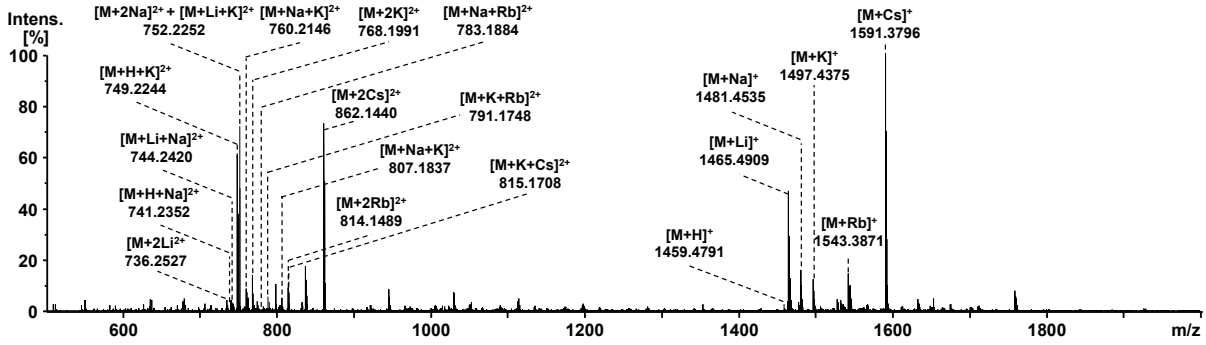

Fig. 1. ESI-MS spectra of G_2-β-CD (1 µM) with mixture of LiCl, NaCl, KCl, RbCl, and CsCl salts (each at 0.3 µM).

3.1 Delineate the influence of usual metals and charge states as discrimination features

3.1.1 Singly charged species

The charge states as well as the number and type of metals can strongly affect the resulting assemblies in terms of size and conformation. TIMS analysis revealed that a clear differentiation between G_1-β-CD/γ-CD and G_2-β-CD/δ-CD couples can be obtained by the addition of a single lithium, sodium, potassium, or cesium ion (Fig. 2-5). The high resolution of TIMS also provides the advantage to estimate the relative content of a given sample by the integration of each ion mobility peak.

Case of G_1-β-CD/γ-CD couple. $[G_1$-β-CD+Li$]^+$ revealed three well resolved peaks with a prominent one at 323.4 Å^2 and two others exhibiting lower intensity at 315.1 Å^2 and 343.6 Å^2 (relative content: 71/21/8, respectively) (Fig. 2A top and Table S1). Moreover, the high resolution (*r*) and resolving power (*R*) give clear evidences that the G_1-β-CD sample can potentially contain a small part of γ-CD, showing a unique peak at 315.1 Å^2 (Fig. 2A bottom and Table S1). Keeping in mind that only a single mobility peak was observed for singly lithiated α-, β- and γ-CD,(Przybylski & Bonnet, 2022) the detection of two or more peaks can be rationally ascribed to distinct positional and/or conformational isomers i.e. stereoisomers and/or conformers, respectively. The adduct with sodium led to three mobility peaks for G_1-β-CD at 318.6, 322.3, and 313.3 Å^2 (47/30/23), respectively (Fig. 2B, top), while a single one at 313.5 Å^2 was observed for γ-CD (Fig. 2B, bottom). The higher peak resolution obtained with sodium confirmed the presence of a few amounts of γ-CD into the G_1-β-CD sample, as previously observed for lithium addition. The introduction of potassium led to four unresolved peaks at 319.3, 316.9, 323.7, and 328.6 Å^2

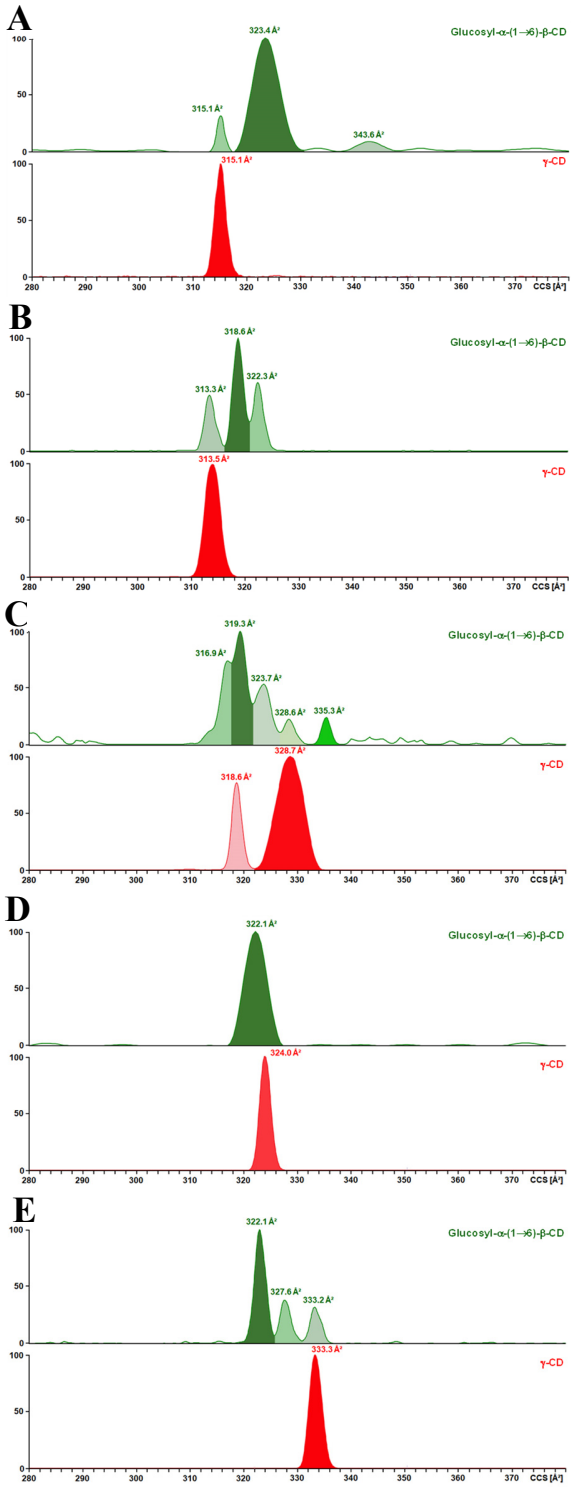

Fig. 2. TIMS based mobilograms and corresponding CCS for singly charged ions of G_1-β-CD (top , green trace) and γ-CD (bottom, red trace) with A) lithium, B sodium, C) potassium, DI) rubidium and E) cesium.

(37/27/19/9) as well as a resolved one at 355.3 Å^2 (8) for G_1-β-CD (Fig. 2C, top), and a couple of CCS at 328.7/318.6 Å^2 (64/36) for γ-CD were detected (Fig. 2C, bottom). Using rubidium showed a unique peak at 322.1 for G_1-β-CD (Fig. 2D, top) and 324.0 Å^2 for γ-CD (Fig. 2D, bottom). The lower R value obtained for G_1-β-CD in the case of rubidium can be attributed to a larger full width at half maximum, suggesting that the peak may contain both G_1-β-CD and γ-CD species. Nonetheless, this impairs to serve as a suitable metal for straightforward discrimination. With cesium, which is the larger cation tested in this work, three quite well resolved peaks were detected for G_1-β-CD at 322.1, 327.6 and, 333.2 Å^2 (59/22/19) (Fig. 2E, top), while a unique one at 333.3 Å^2 occurred for γ-CD (Fig. 2E, bottom). Conversely, protonated G_1-β-CD led to a unique mobility peak corresponding to a CCS of 316.8 Å^2, whereas at least two unresolved peaks, with the most intense at 324.1 Å^2 and a lower one at 317.2 Å^2 were detected for γ-CD (Fig. S1). Based on the standard deviation values (Table S1), the latter peak could be putatively ascribed to G_1-β-CD, which appears as a minor trace in the γ-CD sample.

Case of G_2-β-CD/δ-CD couple. Concerning singly lithiated species of both G_2-β-CD and δ-CD, two distinct couples of peaks were detected at 348.3 Å^2/322.4 Å^2 (Fig. 3A, top) and 353.3 Å^2/332.2 Å^2 (Fig. 3A, bottom). For such couples, the relative content is 99/1 for the former and 82/18 for the latter. Conversely, regarding G_2-β-CD/δ-CD couple no trace of G_2-β-CD was detected in the δ-CD sample. Similarly to lithium adduct, following the complexation with sodium, two couple of peaks were clearly observed both for G_2-β-CD and δ-CD at 347.5/319.6 Å^2 (23/77) (Fig. 3B, top) and 354.0/337.2 Å^2 (48/52) (Fig. 3B, bottom), respectively.

However, in the case of G_2-β-CD, no return to the baseline occurred between the two peaks,

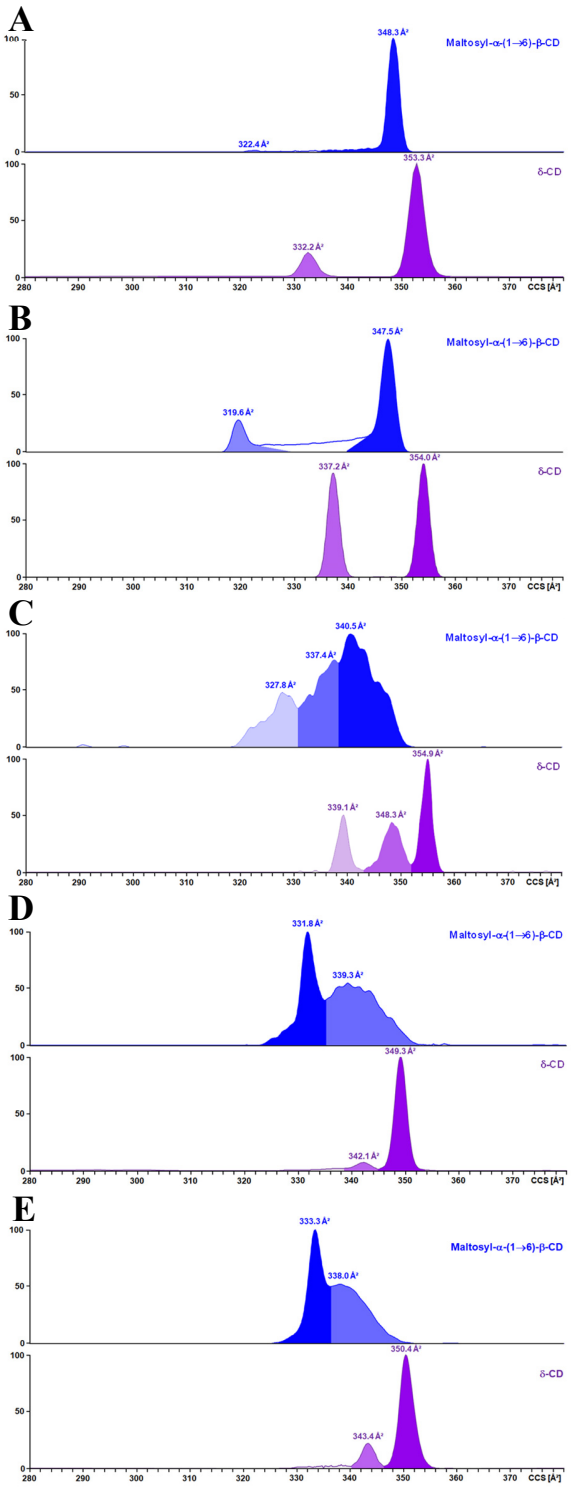

Fig. 3. TIMS based mobilograms and corresponding CCS for singly charged ions of G_2-β-CD (top, blue trace) and δ-CD (bottom, purple trace) with A) lithium, B sodium, C) potassium, DI) rubidium and E) cesium.

indicating a non-equilibrium state and the possible presence of intermediary species. Such phenomenon, also observed to in a less extent for $[G_2\text{-}\beta\text{-CD+Li}]^+$ is similar to an exponential bridge smoothly merging two peaks already described in capillary electrophoresis.(Cherney et al., 2011) Regarding $[G_2\text{-}\beta\text{-CD+K}]^+$, three unresolved peaks could be deducted at ≈327.8, 337.4, and 340.5 $Å^2$ (22/34/44) (Fig. 3C, top), while for $[\delta\text{-CD+K}]^+$, three well resolved ones at 354.9, 348.3 and 339.1 $Å^2$ (24/27/49) are distinguished (Fig. 3C, bottom). The mobilogram of $[G_2\text{-}\beta\text{-CD+Rb}]^+$ revealed a clear peak at 331.8 $Å^2$ and an only partially resolved distribution with a dumbbell shape centred around 339.3 $Å^2$ (Fig. 3D, top), while $[\delta\text{-CD+Rb}]^+$ exhibited two close but resolved peaks at 349.3 (93 %) and 342.1 $Å^2$ (7 %) (Fig. 3D, bottom). Unfortunately, the mobility range of $[G_2\text{-}\beta\text{-CD+Rb}]^+$ is too broad, encompassing the values obtained for δ-CD and preventing a clear conclusion regarding the presence or absence of δ-CD trace in the G_2-β-CD sample. $[G_2\text{-}\beta\text{-CD+Cs}]^+$ and $[\delta\text{-CD+Cs}]^+$ species with CCS couple of 333.3/338.0 $Å^2$ (67/33) (Fig. 3E, top) and 350.4/343.4 $Å^2$ (17/83) (Fig. 3E, bottom), respectively, showed similar behaviour to their corresponding rubidium adduct counterparts.

Regarding both protonated G_2-β-CD and δ-CD, a single peak was observed at 345.2 $Å^2$ and 350.0 $Å^2$, respectively (Fig. S1). As other neutral polyols, CDs present a weak affinity for protons, leading to quite low abundance and sometimes to more of one peak. This is due to the proton mobility and the absence of a unique and stable attachment site (Przybylski et al., 2015; Przybylski & Bonnet, 2022), demonstrating that singly protonated state is not a straightforward reference herein. Singly charged species with lithium and sodium allow us to unambiguously differentiate each

content of the two isomeric couples G_1-β-CD/γ-CD and G_2-β-CD/δ-CD, as well as the identification of trace amounts of a specific structural isomer in other samples or the discovery of new conformers. Nevertheless, with larger alkali metals like potassium, rubidium and cesium, more contrasted results were obtained. Indeed, with such metals, analysis of G_1-β-CD and G_2-β-CD led to a large unresolved peak distribution. The occurrence of various conformations, which may or may not be consecutive to the unique attachment sites of metal-based cations, could explain this observation. To verify such an assumption, doubly charged species with either the two same cations or different ones were investigated.

3.1.2 Homocationic doubly charged species

While the use of two cations generally led to higher CCS values, it was often accompanied by a decrease in *R* and *r*, which ranged from minor to substantial (Fig. 4-5, Table S2).

Case of G_1-β-CD/γ-CD couple. Ternary complexes involving two lithium, led to a well resolved couple peaks at CCS of 348.9/338.1 $Å^2$ for G_1-β-CD (Fig. 4A, top), while a single peak with a CCS equal to 379.9 $Å^2$ occurred for γ-CD (Fig. 4A, bottom). Regarding doubly sodiated species, three partially resolved peaks occurred for G_1-β-CD including two with high intensity at 365.3 (57 %) and 354.0 $Å^2$ (40 %) and a very low one at 346.0 $Å^2$ (3 %) (Fig. 4B, top), while a prominent one at 364.9 $Å^2$ (98 %) with a slight shouldering at 354.5 $Å^2$ (2 %) takes place for γ-CD (Fig. 4B, bottom). As compared to singly potassied G_1-β-CD, the corresponding doubly charged species including two potassium, yielded clearer mobilogram traces, where three quite resolved peaks were observed at 359.3/371.6/350.0 $Å^2$ (59/29/12) (Fig. 5C, top). $[γ\text{-CD}+2K]^{2+}$ exhibited a couple of main peaks at 366.4/349.8 $Å^2$ (45/41) and a less abundant one at 358.2 Å (15 %) (Fig. 5C,

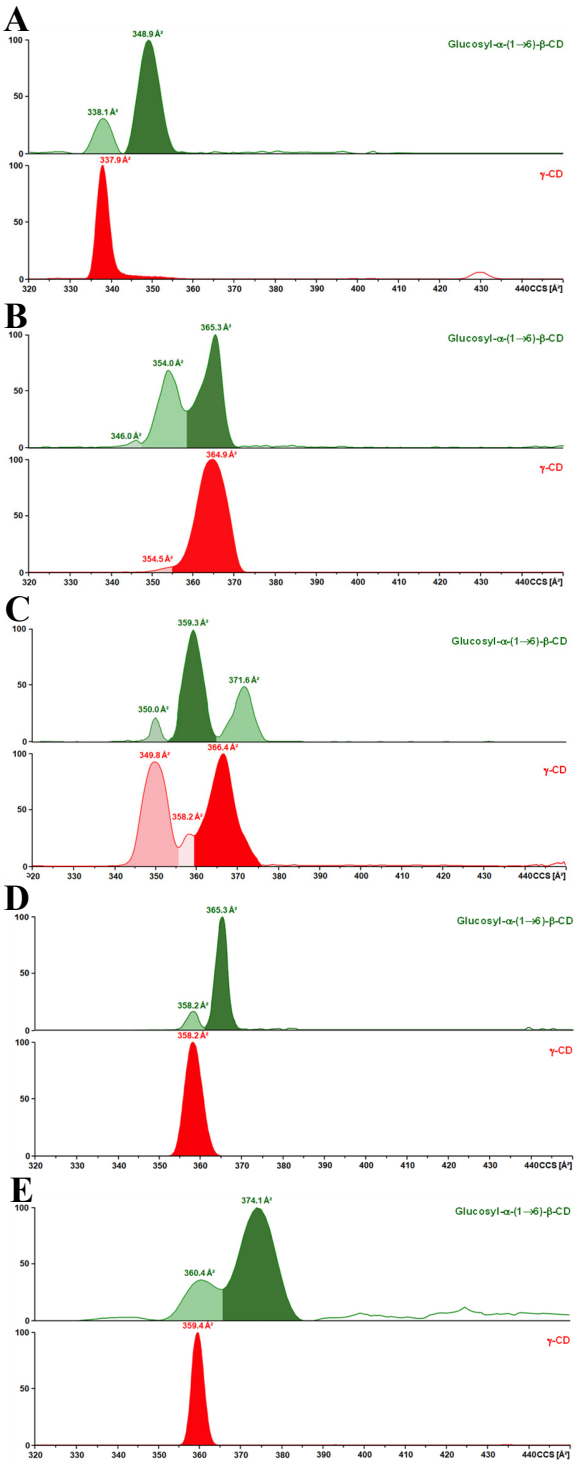

Fig. 4. TIMS based mobilograms and corresponding CCS for homocationic doubly charged ions of G_1-β-CD (top, green trace) and γ-CD (bottom, red trace), with A) lithium, B) sodium, C) potassium, D) rubidium and E) cesium.

387 bottom). Similarly, at the difference of the corresponding singly charged species, the introduction
388 of two rubidium with G_1-β-CD yielded two well resolved peaks with a CCS value of 365.3 $Å^2$ (86
389 %) and 358.2 $Å^2$ (14 %) (Fig. 4D, top), while a unique one is present at 358.2 $Å^2$ for γ-CD (Fig. 4D,
390 bottom). With two cesium, a quite close behaviour to two rubidium complexes was observed. In
391 detail, two large and partially resolved peaks at 374.1 and 360.4 $Å^2$ (71/29) occurred for [G_1-β-
392 CD+2Cs]$^{2+}$ (Fig. 4E, top), while only a narrow peak at 359.4 $Å^2$ was present for [γ-CD+2Cs]$^{2+}$ (Fig.4E,
393 bottom). Careful examination of CCS values both for singly and doubly charged ions with a given
394 cation unambiguously confirmed the presence of γ-CD in the G_1-β-CD sample.

395 *Case of G_2-β-CD/δ-CD couple*. As observed for their singly lithiated counterpart, complex-
396 ation of G_2-β-CD with two lithium led to two well resolved peaks at 383.1/358.1 $Å^2$ (54/46) for
397 G_2-β-CD (Fig. 5A, top), while unresolved ones were obtained at 371.3/385.2 $Å^2$ (83/17) for δ-CD
398 (Fig. 5A, bottom). The same trend was observed for [G_2-β-CD+2Na]$^{2+}$ where a couple of distant
399 peaks were clearly observed with major/minor abundance at 358.7/384.4 $Å^2$(95/5) (Figure 5B,
400 top). For δ-CD, a main and large peak at 374.4 $Å^2$ (78 %) and two lower unresolved ones at
401 386.8/390.3 $Å^2$ (11/11) were detected (Fig. 5B, bottom). Moreover, contrary to their correspond-
402 ing singly charged species, a complete return to the baseline occurred between the two peaks
403 from [G_2-β-CD+2Li]$^{2+}$ and [G_2-β-CD+2Na]$^{2+}$. That suggests the existence of two well distinct and
404 stabilized structures. As quoted out for G_1-β-CD/γ-CD couple, simultaneous complexation of two
405 potassium tends to simplify the mobilogram traces. Indeed, three quite resolved peaks at
406 363.4/372.8/383.3 Å2 (Fig. 5C, top) were present for [G_2-β-CD+2K]$^{2+}$, while [δ-CD+2K]$^{2+}$ led to a
407 major peak at 378.7 $Å^2$ (65 %) and two others ones with both lower abundance and weak

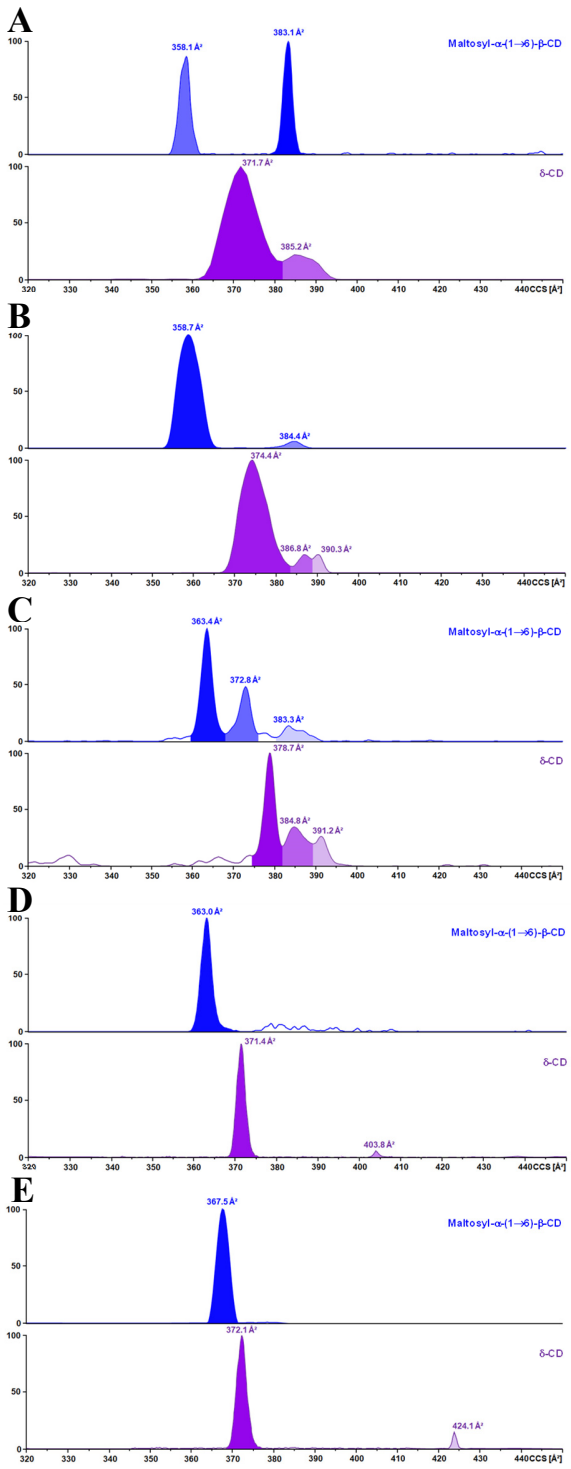

Fig. 5. TIMS based mobilograms and corresponding CCS for homocationic doubly charged ions of G_2-β-CD (top, blue trace) and δ-CD (bottom, purple trace) with A) lithium, B) sodium, C) potassium, D) rubidium and E) cesium.

452 resolution at 384.8 (19 %) and 391.2 Å^2 (17 %) (Fig. 5C, bottom). Regarding [G_2-β-CD+2Rb]$^{2+}$, a
453 single peak was detected at 363.0 Å^2 (Fig. 5D, top), while for δ-CD a largely prominent one at
454 371.4 Å^2 (96 %), and a very minor one at 403.8 Å^2 (4 %) (Fig. 5D, bottom) were found. The same
455 conclusion can be drawn from the doubly cesiated species, where only one peak was detected at
456 367.5 Å^2 for [G_2-β-CD+2Cs]$^{2+}$ (Fig. 5E, top), and a couple of peaks at 372.1/424.1 Å^2 (85/15) for
457 [δ-CD+2Cs]$^{2+}$ (Fig. 5E, bottom). The results on the doubly charged G_2-β-CD/δ-CD couple, con-
458 firmed that there is no clear evidence of the presence of δ-CD in the G_2-β-CD sample.

459 *3.1.3 Heterocationic doubly charged species*

460 Considering heterocationic doubly charged species, i.e. complexes involving one cy-
461 clodextrin with two different cations (Table S2), some observations can be done: i) None ion as-
462 cribed to [CD+Li+X]$^{2+}$ or [CD+H+Y]$^{2+}$ (where X = H, Rb or Cs and Y = Li, Rb or Cs), was detected for
463 the four analysed samples, ii) all obtained CCS values are not necessarily included between those
464 of their corresponding homocationic doubly charged analogues ([CD+X+Y]$^{2+}$ compared to
465 [CD+2X]$^{2+}$ and [CD+2Y]$^{2+}$, where X and Y are two different cations), iii) the number of detected
466 CCS can be different of their corresponding homocationic doubly charged counterparts (Table S2
467 and Figs. S3-S4). The observed results can be explained by the high mobility and weak proton
468 affinity of CDs, as well as by the conformational changes induced by the attachment of lithium,
469 rubidium, and cesium ions to the CDs. Additionally, the nonlinear variations in CCS values be-
470 tween homo- and heterocationic doubly charged series with similar cations could be due to in-
471 creased rigidity or flexibility of both the main rim and any branched α(1→6) glucose/maltose.
472 This would be possibly driven by a first attachment of a given cation, before a second occurred.

Anyway, several distinct cases can be observed. For example, doubly sodiated G_2-β-CD resulted in two different conformations each featuring a sodium stabilized by the primary rim. The second sodium was located either adjacent to the primary rim and the branched maltose or at the non-reducing end of this last one at 358.7 (95 %) and 384.4 $Å^2$ (5 %), respectively (Fig. 6A).

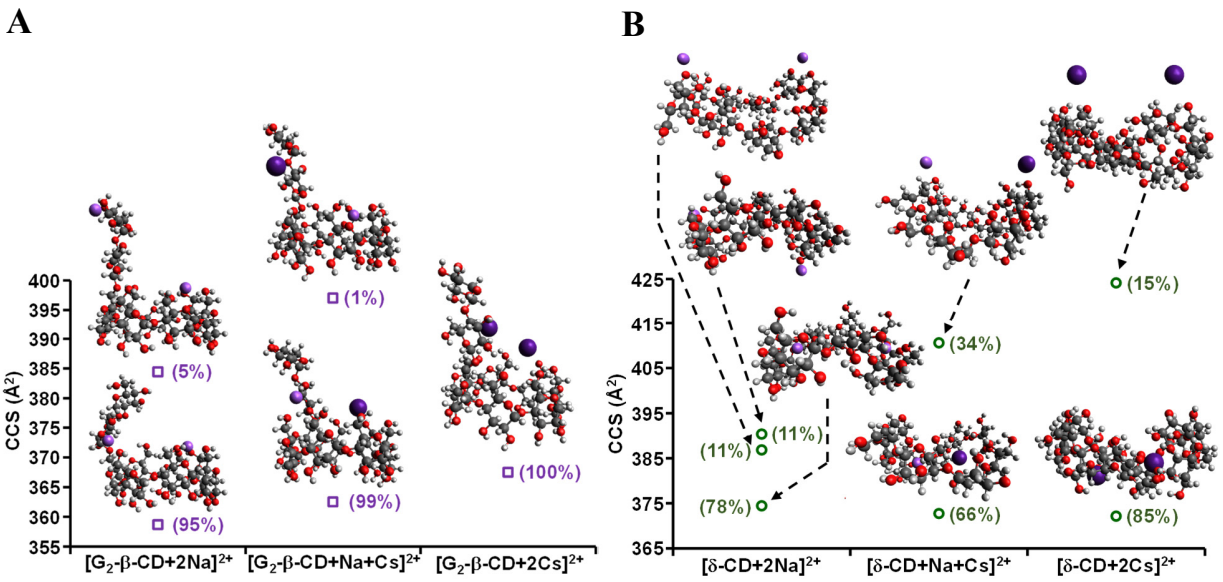

Fig. 6. Evolution of CCS and ascribed theoretical conformations of doubly charged species $[CD+2Na]^{2+}$, $[CD+Na+Cs]^{2+}$ and $[CD+2Cs]^{2+}$ for A) G_2-β-CD (violet square) and B) δ-CD (green circle). The number in brackets indicates the relative content of each supposed conformation.

The formation of a supramolecular complex comprising a sodium and a cesium resulted in the emergence of two distinct conformations. It involves a first cation stabilized by the primary rim and a second one by the grafted maltose backbone leading to the corresponding couples Cs/Na at 362.5 $Å^2$ (99 %) and Na/Cs at 397 $Å^2$ (1 %), respectively. Regarding $[G_2$-β-CD+2Cs$]^{2+}$, a unique peak was observed at 367.5 $Å^2$. Such CCS value was ascribed to a single but a lesser stable conformation than previous ones, emphasizing some limits in accommodation of both CD rim and branched maltose, portraying the difficulty to successfully form and detect complex involving

two cesium ions. Conversely, the presence of two both flipped linkages and twisted rings in the δ-CD confers a high degree of conformational flexibility, enabling the observation of three distinct peaks corresponding to doubly sodiated forms at 374.4 $Å^2$ (78 %), 376.8 $Å^2$ (11 %) and, 390.3 $Å^2$ (11%), respectively (Fig. 6B). Following the previous order, the three potential conformers can be basically described as functions of the position of the two sodium with respect to δ-CD such as: centre-centre, top-top, and top-bottom, respectively. The substitution of one sodium by a larger ion such as cesium ($[δ\text{-CD+Na+Cs}]^{2+}$), still led to a structural rearrangement entailing only two peaks at 372.7 $Å^2$ (66 %; centre-centre) and 410.6 $Å^2$ (34 %; top-top). It can be quoted out that the most abundant peak (centre-centre) matches very well with a more compact structuration than for the three observed $[δ\text{-CD+2Na}]^{2+}$ ions. This output suggests that the CCS of the supra-molecular complex is not solely determined by the size of the cation, but also by the CD's capacity to accommodate optimal template. This assumption is supported by the results from the doubly cesiated ions, where a major peak (85 %) exhibits a slightly smaller CCS at 372.1 $Å^2$ (centre-centre) than the heterocationic sodiated/cesiated analogues. On the other hand, a lower intense peak at 424.1 $Å^2$ (15 %; top-top) was also detected. Hence, the aforementioned hypothesis which can explain the difference in the number of detected CCS based peaks between hetero- and homo-cationic doubly charged species, can also be valid for the comparison between some homoca-tionic doubly charged species, and their singly charged analogues. For example, with the smaller alkali metal studied herein, the singly lithiated G_2-β-CD showed a main peak at 348.3 $Å^2$ (99 %) and a minor peak with a more compact structure at 322.4 $Å^2$ (1 %) (Fig. 7A). Structurally, lithium is stabilized in both cases by three contact points with oxygen from the primary rim. The only

slight difference between the two peaks is that in the minor peak lithium is more centred at the top of the deformed cavity and additionally stabilized by the primary oxygen from the bending of the maltose chain.

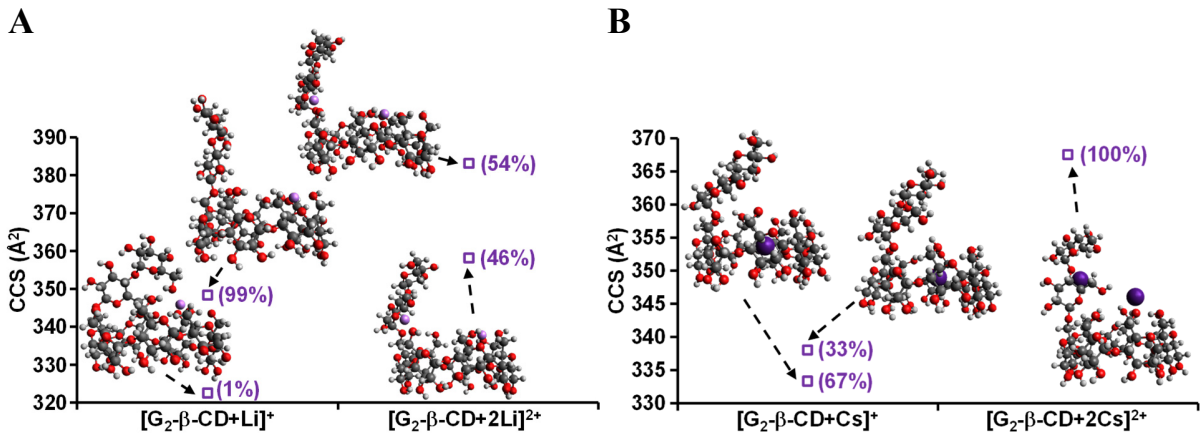

Fig. 7. Evolution of CCS and ascribed theoretical conformations of G_2-β-CD (violet square) as singly and doubly species with A) lithium and B) cesium. Number in brackets indicates the relative content of each supposed conformation.

A more contrasted picture from the bending of the maltose chain was obtained with $[G_2$-β-CD+2Li$]^{2+}$, with two peaks highlighting a balanced content at 358.1 Å^2 (46 %) and 383.1 Å^2 (54 %). In the first case, one lithium is centred at the top of the deformed cavity and the second at the linkage between the CD core and orthogonal orientated maltose. In the second case, a similar structuration occurred, but with lesser inwardly curved maltose. In any case, lithium is stabilized by three proximal oxygens of the rim, as well as an additional oxygen located opposite to the linkage between CD core and maltose. Considering the largest metal, i.e. cesium, $[G_2$-β-CD+Cs$]^+$ ion yielded two distinct CCS at 333.3 Å^2 (67 %) and 338.0 Å^2 (33 %), while $[G_2$-β-CD+2Cs$]^{2+}$ exhibited a unique peak at 367.5 Å^2 (Fig. 7B). For singly charged ions, cesium was centred in the more or less deformed cavity linked to a bent maltose chain, while for doubly charged ions, one cesium

is located at the top of the deformed cavity and the second cesium is stabilized by a maltose chain that is both twisted and bent.

3.2 Differentiation of isomers according to metalation

3.2.1 Discrimination of structural isomers

Considering complexes with the following stoichiometry CD:number of metals, previous studies have shown that, as either the larger the size of the CDs (from α-, β- to γ-CD (Przybylski & Bonnet, 2022), or the higher the methylation degree on β-CD (Przybylski et al., 2015), the higher the proportion of 1:2 complexes relative to 1:1 complexes increased. This is consistent with the results observed in the current study, which indicate that the proportion of 1:2 complexes relative to 1:1 complexes increases continuously from γ-CD to δ-CD and from G_1-β-CD to G_2-β-CD, as evidenced by the sum of the relative intensities observed by MS for all alkali metal cation-based CDs. Nonetheless, contrasted results were obtained regarding the trends for the isomeric couples i.e. G_1-β-CD/γ-CD and G_2-β-CD/δ-CD (Table S1-S2). For the former couples, lithium, sodium and cesium are suitable to unambiguously discriminate any singly charged structural isomers. Of particular interest, high-resolution *r* (1.4-1.7, Table S1) analysis revealed the presence of a small proportion of γ-CD in the G_1-β-CD sample. Conversely, potassium and rubidium did not give a satisfactory resolution to differentiate the two structural isomers and, consequently are not appropriate for such purpose. Due to overlapping peaks, it was not possible to unambiguously identify the first CCS of G_1-β-CD from that of γ-CD (318.6 $Å^2$) when using potassium as the alkali metal cation (Fig. 2C). With rubidium, the unique peak from G_1-β-CD sample resulted in a

563 peak width that was too large to allow a clear identification of the dedicated CCS value of γ-CD,
564 as previously mentioned (Fig. 2D). Regarding the latter couple, G_2-β-CD/δ-CD, only lithium and
565 sodium produced satisfactory results in differentiating the two peaks from G_2-β-CD or δ-CD, with
566 *r* values of 1.3-1.8 and 1.4-3.8, respectively (Fig. 3). Due to a large number of unresolved peaks,
567 potassium, rubidium and cesium can only be used to partially highlight differences between G_2-
568 β-CD and δ-CD. Indeed, this can be achieved merely by taking into account the lower and higher
569 CCS, respectively. Therefore, only the following alkali metal cation pairs provide sufficient differ-
570 entiation between G_2-β-CD and δ-CD: 327.8/354.9 $Å^2$ (*r*: 4), 331.8/349.8 $Å^2$ (*r*: 3.7) and
571 333.3/350.4 $Å^2$ (*r*: 3.3) for potassium, rubidium and cesium, respectively (Fig. 3).

572 At a glance, the mobilograms issued from the simultaneous presence of two identical cat-
573 ions within the various CD complexes tend to reduce the diversity of possible structures and thus,
574 clarify the distribution of the CCS based peaks (Fig. 6). This could be attributed to a higher likeli-
575 hood of certain stabilized structures occurring. Most of herein investigated homocationic doubly
576 charged ions support an easier differentiation of the two CD couples compared to their singly
577 charged analogues, as attested by the CCS values. Nonetheless, regarding the deducted mobility
578 resolution, a more contrasted conclusion can be drawn. Hence, according to a given alkali metal
579 *r* values were between 0.7-1.5 and 0.5-3.1 for G_1-β-CD/γ-CD (Fig. 4) and G_2-β-CD/δ-CD (Fig. 5),
580 respectively. Altogether, the aforementioned data have clearly demonstrated that the ability to
581 efficiently discriminate structural isomers of cyclodextrins must be grasped according to both (i)
582 the given metal, (ii) the number of adducted metals, and of course, (iii) the considered isomers
583 couple. Interestingly, we noted that lithium and sodium seem to be most suitable for both G_1-β-

584 CD/γ-CD and G_2-β-CD/δ-CD couples as well as both singly and homocationic doubly charged spe-
585 cies. Regarding resolution, G_1-β-CD/γ-CD with lithium/sodium, *r* is 1.7/1.4 and 0.9/1.3 for singly
586 and homocationic doubly charged species, respectively, while for G_2-β-CD/δ-CD, *r is* 1.7/1.4 and
587 0.9/1.3 for singly and homocationic doubly charged species, respectively. In addition, the good
588 to high resolution *r* (0.3-6.4) through a given mobilogram, offers, most of the time, the possibility
589 to estimate the relative content of each species in a given sample. Hence, once the peaks that
590 may correspond to structural isomers have been identified, it is necessary to determine the iden-
591 tity of those remaining. In this sense, the hypothesis of the presence of conformational isomers
592 must be investigated.

593 ***3.2.2 Revealing the presence of conformers***

594 If the observation of the profound effect from the charge site on an ion's gas-phase be-
595 haviour i.e. distinct protonation site isomers, the well-known protomers, is very well described
596 for proteins and peptides by ion mobility, the influence of cationization sites on cyclic oligosac-
597 charide structure remains quite under-investigated. The glucopyranose units within CDs are very
598 flexible as a consequence of the rotation and rapid proton exchange of the primary and second-
599 ary hydroxyl groups, and the C5-C6 bond shows a high degree of rotation, which can be also
600 supported to some extent by the glycosidic bond rotation. These intrinsic characteristics involve
601 that many conformers can co-exist, especially in equilibrium in an aqueous solution, as investi-
602 gated by theoretical studies (Gamboa-Carballo et al., 2017; Lipkowitz, 1998). Except for potas-
603 sium, γ-CD exhibits only one peak with all other studied metals suggesting that only one con-
604 former can be detected. Conversely, considering G_1-β-CD analysis, and excluding peaks that may

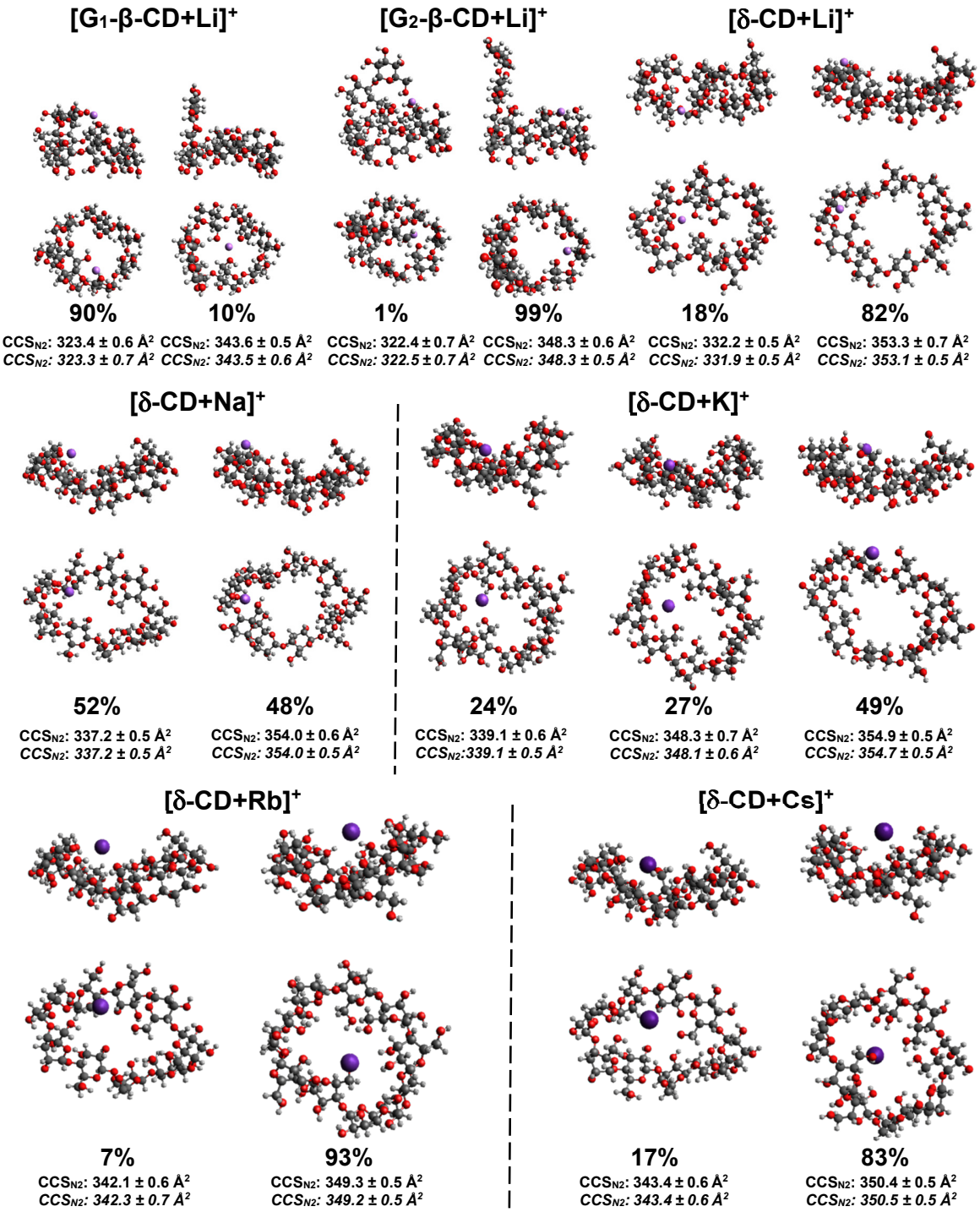

Fig. 8. Side and top views of potential CD/alkali metal structures-based conformers obtained by theoretical approaches and matching with experimental CCS. The estimated content was given below each structure (%) as well as the experimental (top, plain) and theoretical (bottom, italic) CCS_{N2} values. Color coding: very light violet; lithium (first row) light to dark violet; sodium, potassium, rubidium and cesium (second and third row), pink; carbon, gray; oxygen, light red; hydrogen, white.

627 be provided by γ-CD traces, singly charged ion yields to two or more peaks (Fig. 1). Molecular
628 modelling computation allowed us to ascribe the experimental CCS values to potential structures.
629 For example, $[G_1\text{-}\beta\text{-CD+Li}]^+$ yielded to two peaks at 323.4 ± 0.6 and 343.6 ± 0.5 $Å^2$ (*r*: 2.1). The
630 former is quite in a closed form (Fig. 5, $[G_1\text{-}\beta\text{-CD+Li}]^+$, 90 %), with grafted glucose unit acting as a
631 bent lid, trapping lithium between it and side oxygens from the primary rim. The latter appears
632 to have an open structure (Fig. 5, $[G_1\text{-}\beta\text{-CD+Li}]^+$, 10 %) where lithium is stabilized at the top centre
633 of the primary rim. In this last arrangement, the side glucose block is perpendicularly oriented to
634 the primary rim, and the secondary rim exhibits a concave distortion. Regarding $[G_2\text{-}\beta\text{-CD+Li}]^+$,
635 the main form, by far, shows a quite perpendicular orientation of the grafted maltose on one side
636 of the primary rim and a stabilization of the cation at the opposite side.

637 In the case of δ-CD, the very high flexibility of the glycosidic backbone allows it to adopt
638 several conformations. Indeed, δ-CD is the first member of the relatively under-investigated
639 large-ring cyclodextrins (LRCD) where both glucose flips and linkage kinks occurred (French &
640 Johnson, 2007; Raffaini & Ganazzoli, 2007; Saenger et al., 1998). Such enhanced degree of free-
641 dom offers the opportunity for a given cation to be stabilized at the primary rim, at a so-called
642 pseudo-secondary rim (designed as such due to the contribution of a flipped glucose unit) or also
643 in the centre of a more compacted structure. For $[\delta\text{-CD+Li}]^+$, the identified structure highlighted
644 that lithium can be located at the primary rim or at a pseudo- secondary rim, with content equal
645 to 82 and 18 %, respectively (Fig. 8, $[\delta\text{-CD+Li}]^+$). Switching from lithium to sodium still leads to
646 two distinct conformations both with sodium located at the primary rim. In the first conformation
647 (Fig. 8, $[\delta\text{-CD+Na}]^+$, 52 %), the cation attachment site at the *n* and *n+1* units resulted from two

flips towards the exterior of the cavity of glucose at the *n-1* and *n+2* positions. This induced a kink of the glycosidic bonds between *n-1*/*n* and *n+1*/*n+2* units, allowing a tight coordination of Na^+ with two primary oxygens (O···Na: 2.187 and 2.207 Å). In the second conformation (Fig. 8, [δ-CD+Na]$^+$, 48 %), the cation was also coordinated at *n* and *n+1* unit, but involved a three-point interaction. To elaborate further, the coordination of sodium in the second conformation involved the two primary oxygens of *n* and *n+1* (2.175 and 2.313 Å), and oxygen from glycosidic bonds between *n* and *n+1* (2.477 Å). This coordination was made possible due to a more pronounced deformation of the cyclodextrin, with glucose at *n+2* and *n-3* flipping towards the interior of the cavity. The observed CD enlargement resulting from the more pronounced deformation of the cyclodextrin strongly supports the higher CCS value of the second conformation compared to the first. With potassium, which presents a higher ionic radius than sodium and lithium (137 versus 99 and 59 pm, respectively), a greater distance between the cation and oxygens is needed to achieve the most stable non-covalent complex. Three distinct conformations were delineated. The less abundant involves three O···K bonds: one secondary oxygen O(1) of the *n* units (2.617 Å), and two primary ones O(6) from *n-2* (2.801 Å) and *n+3* (2.756 Å) which both own two glucose units tilted by ~ 90° towards the interior of the cavity (Fig. 8, [δ-CD+K]$^+$, 24 %). The second one is only slightly more intense than the first one, and also stabilized by three-points interaction as O(1) of the *n* units (2.572 Å), and two O(6) from *n-1* (2.815 Å) and *n+3* (2.688 Å) both also exhibiting bent glucose towards the cavity's centre (Fig. 8, [δ-CD+K]$^+$, 27 %). The prominent conformation, exhibiting the highest CCS, was ascribed to an extended boat shape. In such an arrangement, potassium is situated within a pocket rich in oxygen at the outer edge of the

669 primary rim, where two closer O(6)···K bonds occur than in the previous structures, originating,
670 from *n* (2.492 Å) and *n+1* (2.616 Å) units (Fig. 8, [δ-CD+K]$^+$, 49 %). Regarding larger cations like
671 rubidium (r_i = 152 pm), two different conformations can be deducted from CCS values. In the
672 minor one, two oxygens from the primary rim from *n* (3.346 pm) and *n+1* (3.710 pm) units inter-
673 act with the cation, while at the exact opposite side of the rim (*n+3*) glucose is again tilted as for
674 [δ-CD+K]$^+$ (Fig. 8, [δ-CD+Rb]$^+$, 7 %). The prominent conformation presents an important distortion
675 of the cavity leading to a quite concave shape. Rubidium was located quite in the bottom centre
676 of the cavity, by bonding at O(1) of *n* unit (3.818 Å), O(2) of *n*+4 (4.039 Å), and two O(6) from *n+3*
677 (3.960 Å) and *n-1* (4.078 Å). The two O(6) involved result again from perpendicularly twisted glu-
678 copyranose (Fig. 8, [δ-CD+Rb]$^+$, 93 %). It must be noted that the examination of CCS values from
679 [δ-CD+Rb]$^+$, shows that a more compact structure occurred for the minor conformation of [δ-
680 CD+Rb]$^+$, than the two less abundant ones from [δ-CD+K]$^+$. On the other hand for the major one,
681 the structure seems to be slightly larger than the aforementioned less abundant [δ-CD+K]$^+$ ion,
682 but more tightened than the main [δ-CD+K]$^+$ complex. Such results strongly suggest a non-negli-
683 gible effect of rubidium as a compacting agent. As for rubidium, the larger alkali metal studied
684 here, cesium (r_i = 167 pm), led to two discernible conformational states. The minor conformation
685 showed a boat shape similar to the prominent [δ-CD+K]$^+$ conformation, but with a smaller CCS
686 value (343.4 versus 354.9 Å^2). Cesium is coordinated to two O(6) from the *n* (3.831 Å) and *n+1*
687 units (4.024 Å) as well as to the hemi-acetal oxygen from *n-1* (4.168 Å), while the *n+3* glucose is
688 tilted towards the interior of the cavity (Fig. 8, [δ-CD+Cs]+, 17 %). Regarding the main confor-
689 mation, the glucose rim adopts a twisted ribbon shape, which is circular in nature, creating a

clamp-like structure with the cation centred in the middle. The unique landscape of the main conformation arises from the rich electron density of the cyclodextrin, which enables multiple interactions. Specifically, the interaction between O(1) and O(2) of the *n* unit (at 3.997 and 4.317 Å, respectively), along with the O(6) of both *n-4* and *n+4* units (at 4.001 and 4.335 Å, respectively), facilitates the centering of the cation in the middle of the deformed cavity. This interaction is further favoured by the twisted glucose units at positions *n-1* and *n+4*, which cause the O(6) groups to orient towards the centre of the cavity.

4. CONCLUSIONS

In this study, we have unambiguously demonstrated that ESI-TIMS-TOF is an effective method for distinguishing positional isomers of macrocyclic carbohydrates, such as cyclodextrins. This capability also provides the opportunity to identify and quantify any residual traces of other isomers, allowing for an estimation of the purity of the investigated sample. However, many pre-cautions must be taken with the choice of the dedicated metal as well as the selected charge state, according to target both resolving power and resolution. As for the CCS values, it is apparent that the CD-metal complexes are not exclusively governed by the size of the cation. Indeed, the presence of not negligible flexibility of the main rim and grafted chain for G_1-β-CD and G_2-β-CD and more enhanced distortion for γ-CD and δ-CD strongly influence the size/shape of the resulting complexes.

In contrast to the smaller CD with quite syn-relative conformations of the glucopyranoside units, γ-CD and δ-CD and larger CD show a high propensity to form band flips and kinks leading to twisted glucose units. These conformers are expected to be in equilibrium in aqueous solution

711 (Lipkowitz, 1998). NMR, which is the reference technique to study conformational changes, is a
712 quite slow spectroscopic technic when compared to the timescale of conformational changes of
713 CDs (Schneider et al., 1998). Indeed, the magnetic pulses are applied to an enormous number of
714 molecules, which means that NMR measurements are averaged over time and space. These lim-
715 itations imply that signals from atoms located at the same position on different glucopyranose
716 units are not distinguished in an NMR spectrum. For this reason, NMR spectra will always lead to
717 symmetrical CDs, which makes this technic not suitable for conformers study. In the present in-
718 vestigation, the use of electrospray coupled with trapped ion mobility mass spectrometry allows
719 to by-pass the short timescale of interconversion, which can preclude the separation of confor-
720 mational isomers in most cases. Such a combination allows us to capture a snapshot portraying
721 the solution. It relies on the sequential “freezing” ability of the molecular state from solution and
722 high resolution separation according to shape/size, as previously demonstrated for carbohydrates
723 and CDs (Przybylski & Bonnet, 2021, 2022; Sastre Toraño et al., 2021). It also seems to be reason-
724 able to assume that the several dozen nanosecond timescales required for potential CD confor-
725 mational switching is compatible with this observation (Gotsev & Ivanov, 2007). For a given ion,
726 the matching of CCS values with molecular modelling approaches, permitted to highlight the pres-
727 ence of several stable conformers. For a more accurate sample characterization, those last results
728 suggest considering not only the CCS value for a given sample, but also the distribution of the
729 resulting peaks pattern. Nonetheless, some pending questions remain, what is the behaviour with
730 higher-valence metals such as transition or noble ones? Is it the type and the location of the cat-
731 ion that induce the various conformation or the prior most adapted conformations which allow

732 the best match attachment of the cation? Also, how many conformers can be distinguished and
733 identified with other grafting locations, such as CD10 and larger?

734 **CONFLICTS OF INTEREST**

735 The authors declare that they have no known competing financial interests or personal
736 relationships that could have appeared to influence the work reported in this paper.

737 **ACKNOWLEDGEMENTS**

738 This work was supported by CEA and the French Ministry of Research and National Re-
739 search Agency as part of the French metabolomics and fluxomics infrastructure (Metab-
740 oHUB, ANR-11-INBS- 0010 grant.

741 **REFERENCES**

742 Abe, J., Hizukuri, S., Koizumi, K., Kubota, Y., & Utamura, T. (1988). Enzymic syntheses of dou-
743 bly branched cyclomaltoheptaoses through the reverse action of Pseudomonas isoamylase.
744 *Carbohydrate Research*, *176*(1), 87-95. https://doi.org/10.1016/0008-6215(88)84060-6
745 Ao, Z., Simsek, S., Zhang, G., Venkatachalam, M., Reuhs, B. L., & Hamaker, B. R. (2007). Starch
746 with a Slow Digestion Property Produced by Altering Its Chain Length, Branch Density,
747 and Crystalline Structure. *Journal of Agricultural and Food Chemistry*, *55*(11), 4540-4547.
748 https://doi.org/10.1021/jf063123x

749 Bansal, P., Yatsyna, V., AbiKhodr, A. H., Warnke, S., Ben Faleh, A., Yalovenko, N., Wysocki,
750 V. H., & Rizzo, T. R. (2020). Using SLIM-Based IMS-IMS Together with Cryogenic In-
751 frared Spectroscopy for Glycan Analysis. *Analytical Chemistry*, *92*(13), 9079-9085.
752 https://doi.org/10.1021/acs.analchem.0c01265
753 Berland, K., Renaud, J. B., & Mayer, P. M. (2014). Utilizing ion mobility and tandem mass spec-
754 trometry to evaluate the structure and behaviour of multimeric cyclodextrin complexes.
755 *Canadian Journal of Chemistry*, *93*(12), 1313-1319. https://doi.org/10.1139/cjc-2014-
756 0419
757 Chakraborty, P., Neumaier, M., Weis, P., & Kappes, M. M. (2023). Exploring Isomerism in Iso-
758 lated Cyclodextrin Oligomers through Trapped Ion Mobility Mass Spectrometry. *Journal*
759 *of the American Society for Mass Spectrometry*, *34*(4), 676-684.
760 https://doi.org/10.1021/jasms.2c00351
761 Chen, Y., Zuo, Z., Dai, X., Xiao, P., Fang, X., Wang, X., Wang, W., & Ding, C.-F. (2018). Gas-
762 phase complexation of α-/β-cyclodextrin with amino acids studied by ion mobility-mass
763 spectrometry and molecular dynamics simulations. *Talanta*, *186*, 1-7.
764 https://doi.org/10.1016/j.talanta.2018.04.003
765 Cherney, L., Kanoatov, M., & Krylov, S. (2011). Method for Determination of Peak Areas in
766 Nonequilibrium Capillary Electrophoresis of Equilibrium Mixtures. *Anal. Chem.*, *83*(22),
767 8617-8622. https://doi.org/10.1021/ac2027113
768 Chouinard, C. D., Nagy, G., Webb, I. K., Garimella, S. V. B., Baker, E. S., Ibrahim, Y. M., &
769 Smith, R. D. (2018). Rapid Ion Mobility Separations of Bile Acid Isomers Using Cyclodex-
770 trin Adducts and Structures for Lossless Ion Manipulations. *Analytical Chemistry*, *90*(18),
771 11086-11091. https://doi.org/10.1021/acs.analchem.8b02990

772 Clowers, B. H., Dwivedi, P., Steiner, W. E., Hill, H. H., & Bendiak, B. (2005). Separation of
773 Sodiated Isobaric Disaccharides and Trisaccharides Using Electrospray Ionization-Atmos-
774 pheric Pressure Ion Mobility-Time of Flight Mass Spectrometry. *Journal of the American*
775 *Society for Mass Spectrometry*, *16*(5), 660-669.
776 https://doi.org/10.1016/j.jasms.2005.01.010
777 Dossmann, H., Fontaine, L., Weisgerber, T., Bonnet, V., Monflier, E., Ponchel, A., & Przybylski,
778 C. (2021). First Steps to Rationalize Host–Guest Interaction between α-, β-, and γ-Cy-
779 clodextrin and Divalent First-Row Transition and Post-transition Metals (Subgroups VIIB,
780 VIIIB, and IIB). *Inorganic Chemistry*, *60*(2), 930-943. https://doi.org/10.1021/acs.inorg-
781 chem.0c03052
782 Erichsen, A., Peters, G. H. J., & Beeren, S. R. (2023). Templated Enzymatic Synthesis of δ-Cy-
783 clodextrin. *J. Am. Chem. Soc.*, *145*(8), 4882-4891. https://doi.org/10.1021/jacs.3c00341
784 Fenn, L. S., & McLean, J. A. (2011). Structural resolution of carbohydrate positional and structural
785 isomers based on gas-phase ion mobility-mass spectrometry. *Physical Chemistry Chemical*
786 *Physics*, *13*(6), 2196-2205. https://doi.org/10.1039/C0CP01414A
787 French, A. D., & Johnson, G. P. (2007). Linkage and pyranosyl ring twisting in cyclodextrins.
788 *Carbohydr. Res.*, *342*(9), 1223-1237. https://doi.org/10.1016/j.carres.2007.02.033
789 French, D., Pulley, A. O., Effenberger, J. A., Rougvie, M. A., & Abdullah, M. (1965). Studies on
790 the Schardinger dextrins : XII. The molecular size and structure of the δ-, ϵ-, ζ-, and η-
791 dextrins. *Archives of Biochemistry and Biophysics*, *111*(1), 153-160.
792 https://doi.org/10.1016/0003-9861(65)90334-6

Gabryelski, W., & Froese, K. L. (2003). Rapid and sensitive differentiation of anomers, linkage, and position isomers of disaccharides using High-Field Asymmetric Waveform Ion Mobility Spectrometry (FAIMS). *Journal of The American Society for Mass Spectrometry*, *14*(3), 265-277. https://doi.org/10.1016/S1044-0305(03)00002-3

Gamboa-Carballo, J. J., Rana, V. K., Levalois-Grützmacher, J., Gaspard, S., & Jáuregui-Haza, U. (2017). Structures and stabilities of naturally occurring cyclodextrins : A theoretical study of symmetrical conformers. *J. Mol. Model.*, *23*(11), 318. https://doi.org/10.1007/s00894-017-3488-4

Gaye, M. M., Kurulugama, R., & Clemmer, D. E. (2015). Investigating carbohydrate isomers by IMS-CID-IMS-MS: precursor and fragment ion cross-sections. *Analyst*, *140*(20), 6922-6932. https://doi.org/10.1039/C5AN00840A

Gotsev, M. G., & Ivanov, P. M. (2007). Large-ring cyclodextrins. A molecular dynamics study of the conformational dynamics and energetics of CD10, CD14 and CD26. *ARKIVOC*, *2007*(13), 167-189. https://doi.org/10.3998/ark.5550190.0008.d20

Harvey, D. J., Seabright, G. E., Vasiljevic, S., Crispin, M., & Struwe, W. B. (2018). Isomer Information from Ion Mobility Separation of High-Mannose Glycan Fragments. *Journal of the American Society for Mass Spectrometry*, *29*(5), 972-988. https://doi.org/10.1021/jasms.8b05810

Hizukuri, S., Abe, J.-I., Koizumi, K., Okada, Y., Kubota, Y., Sakai, S., & Mandai, T. (1989). Hydrolysis and synthesis of branched cyclomaltohexaoses with Pseudomonas isoamylase. *Carbohydrate Research*, *185*(2), 191-198. https://doi.org/10.1016/0008-6215(89)80034-5

814 Hofmann, J., Hahm, H. S., Seeberger, P. H., & Pagel, K. (2015). Identification of carbohydrate
815 anomers using ion mobility–mass spectrometry. *Nature*, *526*(7572), 241-244.
816 https://doi.org/10.1038/nature15388
817 Huang, Y., & Dodds, E. D. (2013). Ion Mobility Studies of Carbohydrates as Group I Adducts :
818 Isomer Specific Collisional Cross Section Dependence on Metal Ion Radius. *Analytical*
819 *Chemistry*, *85*(20), 9728-9735. https://doi.org/10.1021/ac402133f
820 Ishizuka, Y., Nemoto, T., Kanazawa, K., & Nakanishi, H. (2004). 1H NMR spectra of branched-
821 chain cyclomaltohexaoses (α-cyclodextrins). *Carbohydrate Research*, *339*(4), 777-785.
822 https://doi.org/10.1016/j.carres.2003.12.021
823 Kfoury, M., Landy, D., & Fourmentin, S. (2018). Characterization of Cyclodextrin/Volatile Inclu-
824 sion Complexes : A Review. *Molecules*, *23*(5). https://doi.org/10.3390/mole-
825 cules23051204
826 Klein, C., Cologna, S. M., Kurulugama, R. T., Blank, P. S., Darland, E., Mordehai, A., Backlund,
827 P. S., & Yergey, A. L. (2018). Cyclodextrin and malto-dextrose collision cross sections
828 determined in a drift tube ion mobility mass spectrometer using nitrogen bath gas. *Analyst*,
829 *143*(17), 4147-4154. https://doi.org/10.1039/C8AN00646F
830 Koizumi, K., Tanimoto (née Utamura), T., Okada, Y., Nakanishi, N., Kato, N., Tagaki, Y., &
831 Hashimoto, H. (1991). Characterization of five isomers of branched cyclomaltoheptaose
832 (β CD) having degree of polymerization (d.p.) = 9 : Reinvestigation of three positional
833 isomers of diglucosyl-β CD. *Carbohydrate Research*, *215*(1), 127-136.
834 https://doi.org/10.1016/0008-6215(91)84013-5

Koizumi, K., Tanimoto, T., Okada, Y., & Matsuo, M. (1990). Isolation and characterization of three positional isomers of diglucosylcyclomaltoheptaose. *Carbohydrate Research*, *201*(1), 125-134. https://doi.org/10.1016/0008-6215(90)84229-N

Koizumi, K., Utamura, T., Sato, M., & Yagi, Y. (1986). Isolation and characterization of branched cyclodextrins. *Carbohydrate Research*, *153*(1), 55-67. https://doi.org/10.1016/S0008-6215(00)90195-2

Kralj, B., Šmidovnik, A., & Kobe, J. (2009, janvier 1). *Mass spectrometric investigations of α- and β-cyclodextrin complexes with ortho-, meta- and para-coumaric acids by negative mode electrospray ionization*. Rapid Communications in Mass Spectrometry; John Wiley & Sons, Ltd. https://onlinelibrary.wiley.com/doi/abs/10.1002/rcm.3868

Larriba, C., & Hogan, C. J. (2013). Ion Mobilities in Diatomic Gases : Measurement versus Prediction with Non-Specular Scattering Models. *The Journal of Physical Chemistry A*, *117*(19), 3887-3901. https://doi.org/10.1021/jp312432z

Lee, S., Wyttenbach, T., & Bowers, M. T. (1997). Gas phase structures of sodiated oligosaccharides by ion mobility/ion chromatography methods. *In Honour of Chava Lifshitz*, *167-168*, 605-614. https://doi.org/10.1016/S0168-1176(97)00105-5

Lee, S.-S., Lee, J., Oh, J. H., Park, S., Hong, Y., Min, B. K., Lee, H. H. L., Kim, H. I., Kong, X., Lee, S., & Oh, H. B. (2018). Chiral differentiation of D- and L-isoleucine using permethylated β-cyclodextrin : Infrared multiple photon dissociation spectroscopy, ion-mobility mass spectrometry, and DFT calculations. *Physical Chemistry Chemical Physics*, *20*(48), 30428-30436. https://doi.org/10.1039/C8CP05617J

Li, H., Bendiak, B., Siems, W. F., Gang, D. R., & Hill, H. H. (2013). Carbohydrate Structure Characterization by Tandem Ion Mobility Mass Spectrometry (IMMS)2. *Analytical Chemistry*, *85*(5), 2760-2769. https://doi.org/10.1021/ac303273z

Lipkowitz, K. B. (1998). Applications of Computational Chemistry to the Study of Cyclodextrins. *Chem. Rev.*, *98*(5), 1829-1874. https://doi.org/10.1021/cr9700179

Liu, Y., & Clemmer, D. E. (1997). Characterizing Oligosaccharides Using Injected-Ion Mobility/Mass Spectrometry. *Analytical Chemistry*, *69*(13), 2504-2509. https://doi.org/10.1021/ac9701344

Loftsson, T., Hreinsdóttir, D., & Másson, M. (2005). Evaluation of cyclodextrin solubilization of drugs. *International Journal of Pharmaceutics*, *302*(1), 18-28. https://doi.org/10.1016/j.ijpharm.2005.05.042

Nag, A., Chakraborty, P., Natarajan, G., Baksi, A., Mudedla, S. K., Subramanian, V., & Pradeep, T. (2018). Bent Keto Form of Curcumin, Preferential Stabilization of Enol by Piperine, and Isomers of Curcumin∩Cyclodextrin Complexes : Insights from Ion Mobility Mass Spectrometry. *Analytical Chemistry*, *90*(15), 8776-8784. https://doi.org/10.1021/acs.analchem.7b05231

Nagy, G., Attah, I. K., Garimella, S. V. B., Tang, K., Ibrahim, Y. M., Baker, E. S., & Smith, R. D. (2018). Unraveling the isomeric heterogeneity of glycans : Ion mobility separations in structures for lossless ion manipulations. *Chem. Commun.*, *54*(83), 11701-11704. https://doi.org/10.1039/C8CC06966B

Okada, Y., Koizumi, K., & Kitahata, S. (1994). Separation and characterization of five positional isomers of trimaltosyl-cyclomaltoheptaose (trimaltosyl-β-cyclodextrin). *Carbohydrate Research*, *254*, 1-13. https://doi.org/10.1016/0008-6215(94)84238-8

879 Przybylski, C., & Bonnet, V. (2021). Discrimination of isomeric trisaccharides and their relative
880 quantification in honeys using trapped ion mobility spectrometry. *Food Chemistry*, *341*,
881 128182. https://doi.org/10.1016/j.foodchem.2020.128182
882 Przybylski, C., & Bonnet, V. (2022). Probing topology of supramolecular complexes between cy-
883 clodextrins and alkali metals by ion mobility-mass spectrometry. *Carbohydr. Polym.*, *297*,
884 120019. https://doi.org/10.1016/j.carbpol.2022.120019
885 Przybylski, C., Bonnet, V., & Cezard, C. (2015). Probing the common alkali metal affinity of
886 native and variously methylated beta-cyclodextrins by combining electrospray-tandem
887 mass spectrometry and molecular modelling. *Phys. Chem. Chem. Phys.*, *17*(29),
888 19288-19305. https://doi.org/10.1039/c5cp02895g
889 Pu, Y., Ridgeway, M. E., Glaskin, R. S., Park, M. A., Costello, C. E., & Lin, C. (2016). Separation
890 and Identification of Isomeric Glycans by Selected Accumulation-Trapped Ion Mobility
891 Spectrometry-Electron Activated Dissociation Tandem Mass Spectrometry. *Analytical*
892 *Chemistry*, *88*(7), 3440-3443. https://doi.org/10.1021/acs.analchem.6b00041
893 Raffaini, G., & Ganazzoli, F. (2007). Hydration and flexibility of α-, β-, γ- and δ-cyclodextrin : A
894 molecular dynamics study. *Chem. Phys.*, *333*(2), 128-134. https://doi.org/10.1016/j.chem-
895 phys.2007.01.015
896 Rashid, A. M., Saalbach, G., & Bornemann, S. (2014). Discrimination of large maltooligosaccha-
897 rides from isobaric dextran and pullulan using ion mobility mass spectrometry. *Rapid Com-*
898 *munications in Mass Spectrometry*, *28*(2), 191-199. https://doi.org/10.1002/rcm.6771

Saenger, W., Jacob, J., Gessler, K., Steiner, T., Hoffmann, D., Sanbe, H., Koizumi, K., Smith, S. M., & Takaha, T. (1998). Structures of the Common Cyclodextrins and Their Larger Analogues Beyond the Doughnut. *Chem. Rev.*, *98*(5), 1787-1802. https://doi.org/10.1021/cr9700181

Samuelsen, L., Larsen, D., Schönbeck, C., & Beeren, S. R. (2022). PH-Responsive templates modulate the dynamic enzymatic synthesis of cyclodextrins. *Chem. Commun.*, *58*(33), 5152-5155. https://doi.org/10.1039/D1CC06554H

Sastre Toraño, J., Aizpurua-Olaizola, O., Wei, N., Li, T., Unione, L., Jiménez-Osés, G., Corzana, F., Somovilla, V. J., Falcon-Perez, J. M., & Boons, G.-J. (2021). Identification of Isomeric N-Glycans by Conformer Distribution Fingerprinting using Ion Mobility Mass Spectrometry. *Chem. Eur. J.*, *27*(6), 2149-2154. https://doi.org/10.1002/chem.202004522

Schneider, H.-J., Hacket, F., Rüdiger, V., & Ikeda, H. (1998). NMR Studies of Cyclodextrins and Cyclodextrin Complexes. *Chem. Rev.*, *98*(5), 1755-1786. https://doi.org/10.1021/cr970019t

Shiraishi, T., Kusano, S., Tsumuraya, Y., & Sakano, Y. (1989). Synthesis of Maltosyl(α1→6)cyclodextrins through the Reverse Reaction of Thermostable Bacillus acidopullulyticus Pullulanases. *Agricultural and Biological Chemistry*, *53*(8), 2181-2188. https://doi.org/10.1271/bbb1961.53.2181

Singh, M., Sharma, R., & Banerjee, U. C. (2002). Biotechnological applications of cyclodextrins. *Biotechnology Advances*, *20*(5), 341-359. https://doi.org/10.1016/S0734-9750(02)00020-4

Song, L. X., Bai, L., Xu, X. M., He, J., & Pan, S. Z. (2009). Inclusion complexation, encapsulation interaction and inclusion number in cyclodextrin chemistry. *Coordination Chemistry Reviews*, *253*(9), 1276-1284. https://doi.org/10.1016/j.ccr.2008.08.011

Sonnendecker, C., Melzer, S., & Zimmermann, W. (2019). Engineered cyclodextrin glucanotransferases from Bacillus sp. G-825-6 produce large-ring cyclodextrins with high specificity. *MicrobiologyOpen*, *8*(6), e00757. https://doi.org/10.1002/mbo3.757

Sonnendecker, C., Thürmann, S., Przybylski, C., Zitzmann, F. D., Heinke, N., Krauke, Y., Monks, K., Robitzki, A. A., Belder, D., & Zimmermann, W. (2019). Large-Ring Cyclodextrins as Chiral Selectors for Enantiomeric Pharmaceuticals. *Angewandte Chemie International Edition*, *58*(19), 6411-6414. https://doi.org/10.1002/anie.201900911

Sonnendecker, C., Wei, R., Kurze, E., Wang, J., Oeser, T., & Zimmermann, W. (2017). Efficient extracellular recombinant production and purification of a Bacillus cyclodextrin glucanotransferase in Escherichia coli. *Microbial Cell Factories*, *16*(1), 87. https://doi.org/10.1186/s12934-017-0701-1

Sugahara, K., Horikawa, M., & Yamagaki, T. (2015). Amino-beta-cyclodextrin Complex Assisted Ionization for Labile Sesamins and their Ion-mobility Separation in ESI Q-TOF MS. *Mass Spectrometry Letters*, *6*(1), 17-20. https://doi.org/10.5478/MSL.2015.6.1.17

Szejtli, J. (1998). Introduction and General Overview of Cyclodextrin Chemistry. *Chemical Reviews*, *98*(5), 1743-1754. https://doi.org/10.1021/cr970022c

Taniguchi, H., & Honnda, Y. (2009). Amylases. In M. Schaechter (Éd.), *Encyclopedia of Microbiology (Third Edition)* (p. 159-173). Academic Press. https://doi.org/10.1016/B978-012373944-5.00130-9

942 Tanimoto, T., Sakaki, T., & Koizumi, K. (1995). Preparation of 61,62-, 61,63-, 61,64-, and 61,65-
943 di-O-(α-d-glucopyranosyl) cyclomalto-octaoses. *Carbohydrate Research*, *267*(1), 27-37.
944 https://doi.org/10.1016/0008-6215(94)00291-M
945 Terada, Y., Yanase, M., Takata, H., Takaha, T., & Okada, S. (1997). Cyclodextrins Are Not the
946 Major Cyclic α-1,4-Glucans Produced by the Initial Action of Cyclodextrin Glucanotrans-
947 ferase on Amylose. *Journal of Biological Chemistry*, *272*(25), 15729-15733.
948 https://doi.org/10.1074/jbc.272.25.15729
949 Terada Yoshinobu, Sanbe Haruyo, Takaha Takeshi, Kitahata Sumio, Koizumi Kyoko, & Okada
950 Shigetaka. (2001). Comparative Study of the Cyclization Reactions of Three Bacterial Cy-
951 clomaltodextrin Glucanotransferases. *Applied and Environmental Microbiology*, *67*(4),
952 1453-1460. https://doi.org/10.1128/AEM.67.4.1453-1460.2001
953 Tester, R. F., Karkalas, J., & Qi, X. (2004). Starch—Composition, fine structure and architecture.
954 *Journal of Cereal Science*, *39*(2), 151-165. https://doi.org/10.1016/j.jcs.2003.12.001
955 Wei, J., Wu, J., Tang, Y., Ridgeway, M. E., Park, M. A., Costello, C. E., Zaia, J., & Lin, C. (2019).
956 Characterization and Quantification of Highly Sulfated Glycosaminoglycan Isomers by
957 Gated-Trapped Ion Mobility Spectrometry Negative Electron Transfer Dissociation
958 MS/MS. *Analytical Chemistry*, *91*(4), 2994-3001. https://doi.org/10.1021/acs.anal-
959 chem.8b05283
960 Xia, L., Bai, Y., Mu, W., Wang, J., Xu, X., & Jin, Z. (2017). Efficient Synthesis of Glucosyl-β-
961 Cyclodextrin from Maltodextrins by Combined Action of Cyclodextrin Glucosyltransfer-
962 ase and Amyloglucosidase. *Journal of Agricultural and Food Chemistry*, *65*(29),
963 6023-6029. https://doi.org/10.1021/acs.jafc.7b02079

964 Xie, C., Li, L., Wu, Q., Guan, P., Wang, C., Yu, J., & Tang, K. (2021). Effective separation of
965 carbohydrate isomers using metal cation and halogen anion complexes in trapped ion mo-
966 bility spectrometry. *Talanta*, *225*, 121903. https://doi.org/10.1016/j.talanta.2020.121903
967 Yamagaki, T., Ishizuka, Y., Kawabata, S., & Nakanishi, H. (1996). Post-source Decay Fragment
968 Spectra of Cyclomalto-octaose and Branched Cyclomalto-hexaose by Matrix-assisted La-
969 ser Desorption/Ionization Time-of-flight Mass Spectrometry. *Rapid Communications in*
970 *Mass Spectrometry*, *10*(15), 1887-1890. https://doi.org/10.1002/(SICI)1097-
971 0231(199612)10:15<1887::AID-RCM773>3.0.CO;2-2
972 Yamagaki, T., & Nakanishi, H. (1999). Influence of acceleration voltages on relative ion intensi-
973 ties in the post-source decay fragmentation of isomeric cyclic oligosaccharides by matrix-
974 assisted laser desorption/ionization time-of-flight mass spectrometry. *Rapid Communica-*
975 *tions in Mass Spectrometry*, *13*(21), 2199-2203. https://doi.org/10.1002/(SICI)1097-
976 0231(19991115)13:21<2199::AID-RCM775>3.0.CO;2-S
977 Yamagaki, T., & Sato, A. (2009). Peak width-mass correlation in CID MS/MS of isomeric oligo-
978 saccharides using traveling-wave ion mobility mass spectrometry. *Journal of Mass Spec-*
979 *trometry*, *44*(10), 1509-1517. https://doi.org/10.1002/jms.1641
980 Yamamoto, M., Yoshida, A., Hirayama, F., & Uekama, K. (1989). Some physicochemical prop-
981 erties of branched β-cyclodextrins and their inclusion characteristics. *International Journal*
982 *of Pharmaceutics*, *49*(2), 163-171. https://doi.org/10.1016/0378-5173(89)90116-6
983 Yang, S., Gu, L., Wu, F., Dai, X., Xu, F., Li, Q., Fang, X., Yu, S., & Ding, C.-F. (2022). The
984 chirality determination of amino acids by forming complexes with cyclodextrins and metal
985 ions using ion mobility spectrometry, and a DFT calculation. *Talanta*, *243*, 123363.
986 https://doi.org/10.1016/j.talanta.2022.123363

Yang, S., Larsen, D., Pellegrini, M., Meier, S., Mierke, D. F., Beeren, S. R., & Aprahamian, I. (2021). Dynamic enzymatic synthesis of γ-cyclodextrin using a photoremovable hydrazone template. *Chem*, *7*(8), 2190-2200. https://doi.org/10.1016/j.chempr.2021.05.013

Zheng, M., Endo, T., & Zimmermann, W. (2002). Enzymatic Synthesis and Analysis of Large-Ring Cyclodextrins. *Australian Journal of Chemistry*, *55*(2), 39-48.

Zheng, X., Zhang, X., Schocker, N. S., Renslow, R. S., Orton, D. J., Khamsi, J., Ashmus, R. A., Almeida, I. C., Tang, K., Costello, C. E., Smith, R. D., Michael, K., & Baker, E. S. (2017). Enhancing glycan isomer separations with metal ions and positive and negative polarity ion mobility spectrometry-mass spectrometry analyses. *Analytical and Bioanalytical Chemistry*, *409*(2), 467-476. https://doi.org/10.1007/s00216-016-9866-4.